ApJ'00, in press, astro-ph/9908126

Steep Slopes and Preferred Breaks in GRB Spectra: the Role of Photospheres and Comptonization

P. Mészáros [1,2] & M.J. Rees[3]

[1]Dpt. of Astronomy & Astrophysics, Pennsylvania State University, University Park, PA 16802
[2]Institute of Theoretical Physics, University of California, Santa Barbara, CA 93106-4030
[3]Institute of Astronomy, University of Cambridge, Madingley Road, Cambridge CB3 0HA, U.K.

ABSTRACT

The role of a photospheric component and of pair breakdown is examined in the internal shock model of gamma-ray bursts. We discuss some of the mechanisms by which they would produce anomalously steep low energy slopes, X-ray excesses and preferred energy breaks. Sub-relativistic comptonization should dominate in high comoving luminosity bursts with high baryon load, while synchrotron radiation dominates the power law component in bursts which have lower comoving luminosity or have moderate to low baryon loads. A photosphere leading to steep low energy spectral slopes should be prominent in the lowest baryon load cases.

Subject headings: Gamma-rays: Bursts - Radiation Mechanisms- Cosmology: Miscellaneous

1. Introduction

The standard fireball shock scenario for gamma ray bursts (GRB) assumes a synchrotron and/or an inverse Compton (IC) spectrum, in good general agreement with a number of observations (Tavani 1996; Cohen *et al.*1997, Panaitescu, Spada & Mészáros 1999). The physical motivation for this scenario is strong; it would indeed be surprising if the expansion of the ejecta from the huge energies inferred in GRB did not lead to shocks, where synchrotron and IC radiation play a significant role. One need only remind oneself of the dominant role of these effects in AGN jets and supernova remnants. However, in a significant fraction of bursts there is evidence in the 1-10 keV range for spectral intensity slopes steeper than 1/3 (photon number slopes flatter than -2/3), as well as in some cases for a soft X-ray excess over the extrapolated power law from higher energies (Preece *et al.*1998, 1999; Crider *et al.*1997, etc.), and this has served as the motivation for considering a thermal (e.g. Liang (1997) or a thermal/nonthermal (Liang *et al.*1999) comptonization mechanism. While an astrophysical model where this mechanism would arise naturally has been left largely unspecified, Ghisellini & Celotti 1999 have pointed out that if internal shocks lead to high compactness parameters and pair formation, this could naturally produce conditions where the pair temperature and the scattering opacity are self-regulated at values favoring comptonization.

There is also a trend in current analyses of GRB spectra indicating that the apparent clustering of spectral break energies in the 50 keV-1 MeV range is not due to observational selection effects (e.g. Preece *et al.*1998; Brainerd *et al.*1998; see however Dermer *et al.*1999a). Models to explain a preferred break physically, e.g. through a Compton attenuation model (Brainerd *et al.*1998) require reprocessing by an external medium whose column density adjusts itself near a few g cm^{-2}. More recently a preferred break has been attributed to the blackbody peak of the fireball photosphere when this occurs at the comoving pair recombination temperature in the accelerating regime, which is blueshifted to the appropriate observer frame energy (Eichler & Levinson 1999), and in this case the Rayleigh-Jeans portion of the photosphere provides a steep low energy spectral slope. To get a photosphere as close in as to occur at the pair annihilation temperature requires an extremely low baryon load outflow; the presence of a high energy power law extending to GeV then requires a separate explanation.

At the other extreme of large baryon load outflows, Thompson (1994) has considered scattering off MHD turbulence in photospheres in the coasting regime, which boosts the adiabatically cooled thermal photons near the photospheric peak up to a larger break energy, leading to canonical energy slopes of 0 and -1 (photon slopes -1 and -2) below and above the break. An alternative scenario is that of Ghisellini & Celotti (1999), who invoke $e^{\pm}$ pair breakdown in high compactness shocks above the photosphere to achieve a self-regulating nonrelativistic lepton temperature and scattering optical depth of order a few, leading to a thermal comptonization spectrum with standardized features. While this does not explain steep low energy slopes it does provide nonthermal spectral energy power laws of slope ~ 0 close to those of synchrotron, as well as a standard temperature which would lead to a preferred break in the observer frame, if the bulk

Lorentz factor is in a narrow range.

In this paper we synthesize and extend some of these ideas within the framework of the standard fireball internal shock model. While in our previous work (e.g. Mészáros , Laguna & Rees 1993, Rees & Mészáros 1994) we considered photospheres and pair formation, their thermal character, the strong uncompensated photosphere redshift in the coasting phase, and the lack of a straightforward way to get from these a power law extending to GeV energies served as compelling arguments for concentrating on the synchrotron and inverse Compton mechanisms. Here we re-examine the relative roles of photospheres and shocks, as well as those of synchrotron, pair breakdown, scattering on MHD waves and comptonization. This leads to a unified picture where both shocks and/or a photosphere with a nonthermal component can provide most of the luminosity, and where the synchrotron and IC mechanisms in shocks provide the primary spectrum or (in high comoving luminosity cases) the trigger for pair breakdown leading to comptonization. We investigate the range of burst model parameters over which different mechanisms come to the fore, and discuss their role in providing flatter or steeper spectral slopes as well as preferred spectral break energies.

2. Fireball Photospheric Luminosity

We assume a fireball wind of total luminosity output $L_o = 10^{52} L_{52} \mathrm{erg\ s^{-1}}$ expanding from some initial radius r_o, which for the sake of argument is normalized to the last stable orbit r_o at three Schwarzschild radii around a non-rotating black hole of mass $M_{bh} = 10\mu_1 M_\odot$, with a corresponding Kepler rotation timescale t_o,

$$\begin{aligned} r_o = &\quad 6GM_{bh}/c^2 = 0.9 \times 10^7 \mu_1 \text{ cm} , \\ t_o = &\quad 2\pi r_o^{3/2} (2GM_{bh})^{-1/2} = 3.25 \times 10^{-3} \mu_1 \text{ s} . \end{aligned} \tag{1}$$

The initial blackbody temperature in electron rest mass units at that radius is

$$\Theta_o = (k/m_e c^2)(L_o/4\pi r_o^2 c \Gamma_o^2 a)^{1/4} = 2.42 L_{52}^{1/4} \mu_1^{-1/2} \Gamma_o^{-1/2} , \tag{2}$$

(or ~ 1.2 MeV) for a $10\mu_1$ solar mass BH and an initial bulk Lorentz factor $\Gamma_o \geq 1$ at r_o. As the optically thick (adiabatic) wind expands with comoving internal energy $\epsilon' \propto n'^{4/3}$, where n' is the comoving baryon number density, the baryon bulk Lorentz factor increases as $\Gamma \propto r$ and the comoving temperature drops $\Theta' \propto r^{-1}$. The $e^\pm$ pairs drop out of equilibrium (Paczyński 1986, 1990) at $\Theta'_p \sim 0.03$ (~ 17 keV), at a radius r_p where the bulk Lorentz factor has grown linearly to a value Γ_p,

$$\frac{r_p}{r_o} = \frac{\Gamma_p}{\Gamma_o} = \frac{\Theta_o}{\Theta_p} = 7 \times 10^1 L_{52}^{1/4} \mu_1^{-1/2} \Gamma_o^{-1/2} . \tag{3}$$

This is the radius of an $e^\pm$ pair photosphere, above which the scattering optical depth is less than unity, unless the wind carries enough baryons to provide an electron scattering photosphere above

r_p. For a wind baryon load $\dot{M}$ parameterized by a dimensionless entropy $\eta = L/\dot{M}c^2$, the baryonic electrons lead to a photosphere larger than equation (3) if $\eta < \eta_p$ (equation [7]). As long as the wind remains optically thick it is radiation dominated and continues to expand as a relativistic gas with $\Gamma \propto r$ (e.g. Shemi & Piran 1990). Clearly Γ cannot exceed $\eta = L_o/\dot{M}c^2$, and for large baryon loads or moderate η this occurs at a saturation radius $r_s/r_o = \eta/\Gamma_o$ (for low loads or large η see however equation [11]). Above the saturation radius, the flow continues to coast with $\Gamma =$ constant equal to the final value achieved at r_s.

An electron scattering photosphere is defined by $\tau'_s = n'Y\sigma_T r_{ph}/\Gamma = 1$, where $n' = (L/4\pi r^2 m_p c^3 \Gamma\eta)$ is the comoving baryon density, Y is the number of electrons per baryon and r/Γ is a typical comoving length. For relatively low values of $\eta < \eta_*$ (defined in equation [5]) the flow remains optically thick above the saturation radius r_s and the photosphere arises in the coasting regime $\Gamma = \eta =$ constant, at a radius $r_{ph} > r_s$, (Rees & Mészáros , 1994, Thompson 1994),

$$\begin{aligned} \frac{r^{>}_{ph}}{r_o} &= \frac{L\sigma_T Y}{4\pi r_o m_p c^3 \eta^3} = 1.3\times 10^6 L_{52}\mu_1^{-1} Y \eta_2^{-3} \\ &= \Gamma_o^{-1}\eta_*(\eta/\eta_*)^{-3} \quad . \end{aligned} \tag{4}$$

Here η_* is the critical value at which $r^{>}_{ph} = r_s$,

$$\eta_* = \left(\frac{L\sigma_T Y \Gamma_o}{4\pi m_p c^3 r_o}\right)^{1/4} \simeq 10^3 (L_{52}\mu_1^{-1} Y\Gamma_o)^{1/4} \ , \tag{5}$$

which is the wind equivalent of the critical η of an impulsive fireball photosphere discussed in Mészáros , Laguna & Rees 1993, labeled there η_m.

For low baryon loads where $\eta > \eta_*$ a baryonic electron photosphere appears in the accelerating portion $\Gamma \propto r$ of the flow at $r_{ph} < r_s$,

$$\begin{aligned} \frac{r^{<}_{ph}}{r_o} &= \left(\frac{L\sigma_T Y}{4\pi r_o m_p c^3 \eta \Gamma_o^2}\right)^{1/3} = 2.35\times 10^3 (L_{52} Y \Gamma_o^{-2})^{1/3} \mu_1^{-1/3}\eta_2^{-1/3} \\ &= \Gamma_o^{-1}\eta_*(\eta/\eta_*)^{-1/3} \quad . \end{aligned} \tag{6}$$

These photospheric radii are shown in Figure 1. For sufficiently high η, the baryon photospheric radius given by equation (6) can formally become smaller than the pair photosphere radius of equation (3), in which case the latter should be used. The minimum possible photospheric radius is therefore achieved at $r = r_p$ given by equation (3), requiring extremely large values of $\eta > \eta_p$ $(> \eta_*)$,

$$\eta_p = 4\times 10^6 L_{52}^{1/4}\mu_1^{1/2} Y \Gamma_o^{-1/2} = 3.75\times 10^3 \eta_*(\mu_1 Y \Gamma_o^{-1})^{3/4} \ , \tag{7}$$

which implies extremely low baryon loads, $\dot{M} \leq 1.5\times 10^{-8} M_\odot \mathrm{s}^{-1}$.

The Lorentz factor attained at the photosphere, Γ_{ph}, grows linearly with η for $1 \leq \eta \leq \eta_*$ (assuming $\Gamma_o = 1$), then it decays as $\eta^{-1/3}$ up to η_p and remains constant above that. The

comoving temperature $\Theta'_{ph} \propto n'^{1/3} \propto r^{-1}$ for a photosphere at $r_{ph} < r_s$, while $\Theta'_p \propto r^{-2/3}$ for $r_{ph} > r_s$. The observer-frame photospheric temperature $\Theta_{ph} = \Theta'_{ph}\Gamma_{ph}$ is then

$$\frac{\Theta_{ph}}{\Theta_o} = \begin{cases} (r_{ph}/r_s)^{-2/3} = (\eta/\eta_*)^{8/3}, & \text{for } \eta < \eta_*,\ r_{ph} > r_s; \\ 1, & \text{for } \eta > \eta_*,\ r_{ph} < r_s. \end{cases} \tag{8}$$

The observed photospheric thermal luminosity is $L_{pht} \propto r^2\Gamma^2\Theta'^4_{ph} \propto r^0$ for $r < r_s$ and $L_{pht} \propto r^{-2/3}$ for $r > r_s$, hence

$$\frac{L_{pht}}{L_o} = \begin{cases} (r^{>}_{ph}/r_s)^{-2/3} = (\eta/\eta_*)^{8/3}, & \text{for } \eta < \eta_*,\ r_{ph} > r_s; \\ 1, & \text{for } \eta > \eta_*,\ r_{ph} < r_s. \end{cases} \tag{9}$$

3. Kinetic and Internal Shock Luminosity

For typical values of $\eta \lesssim 10^3$ it is clear that the terminal baryon Lorentz factor is $\Gamma = \eta$, since the photosphere occurs beyond the saturation radius after the baryons are already coasting with η. However the terminal baryon Lorentz factor is less obvious in cases where $\eta > \eta_*$. For such values, a photosphere occurs in the regime where $\Gamma \propto r$, so $r_{ph} < r_s$, but the question is what happens to the baryons above this photosphere, and what is the appropriate value of r_s. One possibility is that the outflow has magnetic fields strong enough that Poynting stresses continue to accelerate baryons outside the photosphere. If radiation provides the dominant relativistic pressure, to achieve a saturation radius at the value $r_s/r_o = \eta/\Gamma_o$ would require the baryons to be coupled to the radiation out to that radius, beyond the photosphere. Alternatively, it is sometimes assumed that the baryons decouple at the photosphere r_{ph}, and coast thereafter with $\Gamma = \Gamma_{ph} = \Gamma_o(r_{ph}/r_o)$. However, the fact that the outflow has become optically thin to scattering means that most photons no longer scatter. Nonetheless, most of the electrons above the photosphere can still scatter with a decreasing fraction of free-streaming photons, as long as the comoving Compton drag time $t'_{dr} = m_pc^2/c\sigma_T u'_\Gamma$ is less than the comoving expansion time $t'_{ex} = r/c\Gamma$. The ratio of these two times,

$$(t'_{dr}/t'_{ex}) = (4\pi m_p c^3 r\Gamma^3/L\sigma_T) = (\eta_*/\Gamma_o)^{-4}(r/r_o)^4 \ , \tag{10}$$

exceeds unity above a radius $r_*/r_o = \eta_*/\Gamma_o$. Thus for $\eta > \eta_*$ the appropriate saturation Lorentz factor is η_* (instead of the larger η) and the saturation radius is $r_s/r_o = r_*/r_o = \eta_*/\Gamma_o < \eta/\Gamma_o$. Thus, in general the terminal bulk Lorentz factor and the saturation radius are

$$\Gamma_s = \min\ [\eta, \eta_*] \quad , \quad (r_s/r_o) = \min\ [\eta, \eta_*]/\Gamma_o \ , \tag{11}$$

where the critical value η_* is given by equation (5).

The observer-frame kinetic (matter) luminosity of the outflow $L_k \propto r^2\Gamma^2 n'(kT' + m_pc^2) \propto r$ for $r < r_s$ and $L_k \propto r^0$ for $r > r_s$. For $\eta < \eta_*$ it is clear that L_k reaches the level $L_o = \dot{M}c^2\eta$ since the terminal bulk Lorentz factor saturates at the initial dimensionless entropy η. However,

for $\eta > \eta_*$ the terminal L_k can only reach a lower level, since the bulk Lorentz factor saturates at the lower value $\eta_* < \eta$. The terminal value of L_k above r_s is then

$$\frac{L_k}{L_o} = \begin{cases} 1 \ , & \text{for } \eta < \eta_*, \ r > r_s; \\ (\eta_*/\eta) \leq 1 \ , & \text{for } \eta > \eta_*, \ r > r_s. \end{cases} \tag{12}$$

Internal shocks can occur when the flow has variations in the initial η or L_o with consequent variations in the terminal Lorentz factors, so shells with different Γ_s catch up with each other. The shocks cannot occur at $r < r_s$ since in this region both shells accelerate at the same rate $\Gamma \propto r$ and do not catch up. After Γ has saturated at $r > r_s$, shocks develop at radii $\sim 2ct_v\Gamma_1\Gamma_2 \sim 2ct_v\Gamma^2$ for shells whose terminal Lorentz factors differ by $\Delta\Gamma = \Gamma_2 - \Gamma_1 \sim \Gamma$ as a result of initial variations in η or L over timescales $t_v = \xi_v t_o < t_w$, where $\xi_v \geq 1$ and t_o is the minimum dynamic timescale in equation (1).

$$(r_{sh}/r_o) = 2.17 \times 10^5 \xi_v \mu_1 \Gamma_2^2 = 2.17 \times 10^1 \xi_v \eta_*^2 (\Gamma/\eta_*)^2 \ . \tag{13}$$

(The factor $21.7 = 2 \times 2\pi \times \sqrt{3}$ comes from the factor $2ct_v$ in the shock radius definition, the 2π from taking the rotation time at r_o rather than crossing time, and $\sqrt{3}$ because r_o is at three Schwarzschild radii.)

To produce non-thermal radiation, shocks must occur in an optically thin region, which requires

$$\eta > \eta_{sh,m} = 1.42 \times 10^2 L_{52}^{1/5} \mu_1^{-1/5} Y^{1/5} \xi_v^{-1/5} \ , \text{ for } r_{sh} > r_{ph}^{>}, \tag{14}$$

in order for a shock to occur above a photosphere which is in the coasting region, $r_{sh} > r_{ph}^{>} > r_s$. For $\xi_v = 10^3$ corresponding to variability timescales $10^3 t_o \sim 1$s, this can be as low as $\eta_{sh,m} \sim 35$. For even higher loads such that $\eta < \eta_{sh,1m}$, the photosphere is further out on the coasting regime, and any shocks would occur inside the photosphere. Internal shock radii are shown in Figure 1 as a function of η for various multiples $\xi_v = t_v/t_o$ of the Kepler time at the last stable orbit t_o. However, from causality considerations shocks may occur at even lower radii, formally corresponding to $\xi_v \geq 1/21.7$, since as soon as the $r > r_s$ coasting regime is reached shells of different η can catch up with each other. This would allow smaller regions where the variability timescale is as small as r_o/c.

For very low baryon loads or very high $\eta > \eta_*$, the photosphere arises in the accelerating region, and in this region shocks are not possible. They are, however, possible beyond $r_s = r_* = r_o \eta_* \Gamma_o^{-1}$, where the baryon Lorentz factor has saturated to the value $\Gamma_s = \eta_*$. Any initial variations on a timescale t_v will lead to shocks at a radius r_{sh} given by equation (13) with $\Gamma_s \sim \eta_*$, which will be located above $r_s = r_*$. There is thus a maximum possible internal shock radius for any given ξ_v,

$$r_{sh,M} = 2.17 \times 10^1 \xi_v \eta_*^2 r_o = 2.17 \times 10^{14} (L_{52} \mu_1 \Gamma_o Y)^{1/2} \xi_v \text{ cm} \ , \tag{15}$$

which, unless ξ_v is large or the external density is very large, can still be smaller than the radius where external shocks are expected. The range where internal shocks can occur is shown as the horizontally or vertically striped region in Figure 1.

The internal shocks in the wind can dissipate a fraction of the terminal kinetic energy luminosity L_k above the saturation radius r_s. For a mechanical efficiency $\varepsilon_{sh} = 10^{-1}\varepsilon_{sh-1}$ of conversion of kinetic energy L_k into random energy which can be radiated, the shock luminosity in the radiative regime is

$$\frac{L_{sh}}{L_o} = \begin{cases} 10^{-1}\varepsilon_{sh-1} \ , & \text{for } \eta < \eta_*, \ r > r_s; \\ 10^{-1}\varepsilon_{sh-1}(\eta/\eta_*)^{-1} \ , & \text{for } \eta > \eta_*, \ r > r_s. \end{cases} \tag{16}$$

4. Photosphere and Shock Spectra: Comptonization and Pair Formation

The basic photospheric spectrum is that of a blackbody, $xF_x \propto x^3 \exp(-x/\Theta_{ph})$, with a thermal peak at

$$x_{ph} \sim 3\Theta_{ph} \leq x_{pho} = 3\Theta_o \ , \tag{17}$$

where Θ_{ph}, Θ_o are given by equations (8,2). Notice that at r_s the level is $L_{pht} = L_o$ and the spectral peak is at $x_{ph} \sim 3\Theta_o \sim 1$, from equations (9) (8). For $r_{ph} > r_s$, both L_{pht} and Θ_{ph} decrease $\propto (r_{ph}/r_s)^{-2/3}$. In an xF_x or xL_x diagram the thermal peak x_{ph} (labeled with T in Figure 2) moves down and to the left with a slope 1 as η decreases. Before leaving the photosphere, however, the blackbody photons can act as seeds for scattering to higher energies, if there is a substantial amount of energy in scattering centers moving with characteristic speeds or energies larger than that of the emitting electrons (which are subrelativistic since $\Theta'_{ph} \leq \Theta'_p = 0.03$). Alfvén waves generated by magnetic field reconnection or MHD turbulence can act as such centers (Thompson 1994). Alfvén waves travel at speeds V_w nearly the speed of light, with an equivalent comoving electron energy $\Theta'_w = kT'_w/m_ec^2 = (1/3)\langle\gamma_w^2 - 1\rangle \simeq (1/3)\langle V_w^2/c^2\rangle \lesssim (1/3)$, where $V_w/c \lesssim 1$, and these waves can be efficiently damped for $\tau_s > 1$. Alternatively, shocks which occur inside the photosphere may also induce Alfvén waves. Repeated scattering on the Alfvén waves acts in the same way as comptonization off hot electrons. The spectrum follows from conservation of photon number and conservation of energy. As seen in the observer frame, starting from seed photons at energy $\Theta_{ph} \leq \Theta_o$ this yields a spectrum $F_x \propto x^0$ or $xF_x \propto x$, as the conserved photon number is scattered up in energy. The photons diffuse up and to the right on a slope $\propto x$ in the xF_x diagram. From conservation of energy, the maximum energy they can reach is $\sim 3\Theta_o \sim 1$. However, if the energy in Alfvén waves or turbulence is a fraction $\epsilon_w < 1$ of the total L_o, the comptonized photosphere luminosity is

$$L_{phc} = \epsilon_w L_o \ , \tag{18}$$

and the comptonized photosphere spectrum $xF_x \propto x$ can extend only up to a break energy

$$x_{phc} = \min[\epsilon_w 3\Theta_o, (L_{phc}/L_{ph})3\Theta_{ph}] \leq 3\Theta_o \ . \tag{19}$$

This is still much less than the wave equivalent energy in the lab-frame, $\Theta_w = (kT'_w/m_ec^2)\eta \lesssim (1/3)\Gamma$. Thus above this break energy, an increasingly smaller fraction of the total photons can be

scattered with spectrum $xF_x \propto x^0$ up to a maximum energy in the lab frame

$$x_w \sim 3\Theta_w \lesssim \Gamma \ . \tag{20}$$

As discussed by Thompson (1994) and in classical references on comptonization, such a spectrum $xF_x \propto x^0$ is naturally expected from the diffusion of photons out of bounded scattering regions (such as reconnection hot-spots or turbulent cells in this case). We show in Figure 2 the comptonized photosphere component (labeled PHC), assuming a turbulent wave energy level $\epsilon_w = 10^{-1} L_o$, for various values of η, while in Figure 3 a lower value $\epsilon_w = 10^{-2}$ is assumed.

Internal shocks outside the photosphere, expected in the coasting regime if the outflow is unsteady, provide a significant nonthermal component of the spectrum. The primary energy loss mechanism in the shocks is synchrotron radiation, or inverse Compton (IC). It is common to assume that at the shocks the magnetic field energy density is some fraction ϵ_B of the equipartition value with the outflow. The dimensionless field at the base of the flow is then

$$x_{Bo} = (B/B_Q) = (2L_o\epsilon_B/r_o^2 c)^{1/2} B_Q^{-1} = 2L_{52}^{1/2}\epsilon_B^{1/2}\mu_1^{-1} \ , \tag{21}$$

where $B_Q = 2\pi m_2^2 c^3/eh = 4.44 \times 10^{13} G$ is the critical field. Thus the dimensionless comoving field at the shock is

$$x'_{Bsh} = x_{Bo}(r_{sh}/r_o)^{-1}\Gamma^{-1} = 10^{-7}\Gamma_2^{-3} L_{52}^{1/2}\epsilon_B^{1/2}\xi_v^{-1}\mu_1^{-1} \ . \tag{22}$$

Note that if the fields are turbulently generated and equipartition is with respect to L_{sh}, instead of L_o, then from equation (16), $\epsilon_B \leq \min[\varepsilon_{sh}, \varepsilon_{sh}(\eta_*/\eta)]$. This is a time average value of B' over the duration of the shocks, and it neglects any time-varying compression factors associated with individual pulses. The observer-frame dimensionless synchrotron peak frequency in units of electron rest mass is $x_{sy} = (3/2)x'_B\gamma_m^2\Gamma$, where the minimum electron random Lorentz factor in internal shocks $\gamma_m \sim 0.9 \times 10^3 \epsilon_e$ is typically a fraction ϵ_e of the equipartition value $0.5 m_p/m_e$, remembering that internal shock collide at relative speeds $\Gamma_{rel} \sim 1$. Thus the observed synchrotron peak is at

$$x_{sy} = x_*(\Gamma/\eta_*)^{-2} = 1.26 \times 10^1 \Gamma_2^{-2} L_{52}^{1/2}\epsilon_B^{1/2}\epsilon_e^2\mu_1^{-1}\xi_v^{-1} \ , \tag{23}$$

where $x_* = 1.26 \times 10^{-1}\epsilon_B^{1/2}\epsilon_e^2\mu_1^{-1/2}(Y\Gamma_o)^{-1/2}\xi_v^{-1}$. The comoving synchrotron cooling time is $t'_{sy} = 2.5 \times 10^{-19} x'^{-2}_B \gamma^{-1} = 2.5 \times 10^{-8}\Gamma_2^6 L_{52}^{-1}\epsilon_B^{-1}\epsilon_e^{-1}\mu_1^2\xi_v^2$ s, using equation (22). For $\epsilon_B \ll 1$ the IC mechanism can become important for the MeV radiation. However, for ϵ_B not too far below equipartition values, the IC losses occur on timescales comparable or longer than synchrotron, and produce photons well above the MeV range where breaks and anomalous slopes occur. The comoving expansion time is $t'_{ex} = r/c\Gamma = 0.65\Gamma_2\mu_1\xi_v$ s, and the ratio t'_{sy}/t'_{ex} exceeds unity only for rather large $\Gamma \gtrsim 3 \times 10^3 L_{52}^{1/5}\epsilon_B^{1/5}\epsilon_e^{1/5}\mu_1^{-1/5}\xi_v^{-1/5}$ if $\gamma \geq \gamma_m$. Thus the electrons are in the radiative regime above the synchrotron break x_{sy} in all cases considered, and also for a large range below it. Above the break x_{sy} the synchrotron spectrum is then $xF_x \propto x^0$, or more generally $xF_x \propto x^{-(p-2)/2}$, from the power law electrons $N(\gamma) \propto \gamma^{-p}$ above $\gamma = 0.9 \times 10^3 \epsilon_e$ produced by Fermi acceleration in the shocks (for the rest of the discussion we assume $p = 2$ or $\propto x^0$ above

the break as an example). Below x_{sy} one has $xF_x \propto x^{1/2}$, down to a synchrotron self-absorption frequency

$$x_a \leq 10^{-4}\Gamma_2^{-4/5}L_{52}^{3/10}\varepsilon_{sh-1}^{2/5}\epsilon_{B-1}^{-1/10}\epsilon_e^{-4/5}\mu_1^{-3/5}\xi_v^{-3/5} \ , \tag{24}$$

where the equality applies if $xF_x \propto x^{1/2}$ down to x_a, and the inequality applies if there is a transition to an adiabatic regime $\propto x^{4/3}$ before reaching x_a (for very high Γ or ξ_v). Schematic synchrotron spectra are shown in Figure 2 from shocks where $\varepsilon_{sh} = 10^{-1}$, and in Figure 3 (left panel) where $\varepsilon_{sh} = 3 \times 10^{-3}$, assuming $p = 2$. These curves, labeled S, show the break at x_{sy} and a radiative slope 1/2 below that down to x_a. For cases where an adiabatic regime is achieved at frequencies below x_{sy} but above x_a, the synchrotron slope would steepen to 4/3 and x_a moves further down in frequency.

Pair breakdown via $\gamma\gamma \to e^{\pm}$ can occur when the comoving synchrotron luminosity from the internal shocks is large enough, which is the case over a non-negligible range of parameter space. The comoving compactness parameter is $\ell' = n'_\gamma \sigma_T (r/\Gamma)$, where $n'_\gamma = (\alpha L_{sh}/4\pi r_{sh}^2 m_e c^3 \Gamma^2)$ is the comoving photon density and α is the fraction above threshold. For typical synchrotron spectra peaking at x_{sy} and with $xF_x \propto x^0$ above that, a fraction above threshold in the comoving frame $\alpha = 0.3\alpha_{-.3}$ is a typical value for the high ℓ' cases. Thus

$$\ell' = (\alpha L_{sh}\sigma_T/8\pi m_e c^3 t_v \Gamma^5) \simeq 3 \times 10^2 \Gamma_2^{-5} L_{52}\varepsilon_{sh-1}\alpha_{-.3}\xi_v^{-1} \ . \tag{25}$$

For values of $\Gamma > \Gamma_{\ell'} \sim 3.1\times10^2(L_{52}\varepsilon_{sh-1}\alpha_{-.3}\mu_1^{-1}\xi_v^{-1})^{1/5}$ the compactness $\ell' \leq 1$ and pair formation does not occur. This corresponds to shock radii $(r_{sh}/r_o)_{\ell'} \geq 0.7 \times 10^8 L_{52}\varepsilon_{sh-1}\alpha_{-.3}\mu_1^{-1}\Gamma_2^{-3}$. Below that, in the range $r_s < r_{sh} < r_{sh\ell'}$, one has $\ell' \gtrsim 1$, and pair breakdown rapidly adds to the opacity and cooling. This leads to a self-regulating pair plasma whose scattering optical depth $\tau_s \sim$ several, with a characteristic mean $e^{\pm}$ energy $\Theta'_c \sim m_e c^2/\tau_s \sim 10^{-1}$ (e.g. Svensson 1987, Ghisellini & Celotti 1999). Clearly, τ_s cannot be too large, otherwise advection and adiabatic cooling would dominate over comptonization and diffusion. At such nonrelativistic energies, cyclotron radiation produces seed photons at harmonics whose energy is much lower than x_{sy}, but repeated scattering on the much hotter $e^{\pm}$ produces a comptonized spectrum $F_{x'} \propto x'^0$ up to the maximum energy Θ'_c. For $\Gamma = \eta$ (and $\ell' > 1$), one then has an observer-frame characteristic break energy

$$x_c \sim 10^{-1}\Gamma \sim 10\Gamma_2 \ , \tag{26}$$

and below that a spectrum $xF_x \propto x$. The pair Comptonized luminosity is comparable to the (initial) synchrotron shock luminosity in the absence of pairs, $L_c/L_o = L_{sh}/L_o$ given by equation (16), since the self-regulation of the comptonizing pair plasma is achieved by a time-averaged balance between energy dissipation by the shocks and radiative losses.

Above the break x_c, one would expect a drop-off of the spectrum, in the absence of other effects. However, since internal shocks occur in the coasting regime and self-regulating pair breakdown tends to maintain a moderate scattering optical depth, reconnection and MHD turbulence may arise here too, leading to Alfvén waves of much higher characteristic energies than that of the pairs, which could lead to a flatter power law spectrum $xF_x \propto x^0$ extending above x_c

up to energies x_w similar to that given in equation (20). In Figure 2 the top row shows cases where $\ell' < 1$ and hence only the photosphere (with thermal T and nonthermal PHC) and the shock synchrotron (S) components are present. The middle row shows the marginal cases where $\ell' = 1$ and hence besides the photosphere T and PHC components one expects the synchrotron S and the pair breakdown comptonized C components to be comparably important. The bottom row of Figure 2 shows cases with $\ell' \gg 1$, where pair breakdown is so important as to completely replace the synchrotron component S with a self-regulated comptonizing pair plasma component C. Both the S and C components have a luminosity level given by a shock efficiency (e.g. Kumar 1999) $\varepsilon_{sh} = 10^{-1}$ in Figure 2, with the effects of a lower value $\varepsilon_{sh} = 3 \times 10^{-3}$ shown in Figure 3 (left).

5. Discussion

Within the framework of the standard internal shock model, we have analyzed the observable effects of the two major radiating regions, the photosphere and the internal shocks, which are expected to contribute to the flux from an unsteady fireball outflow model of GRB. Note that, as in most GRB models, the spherically symmetric assumption applies to any conical outflow whose opening half-angle is $\gtrsim \Gamma^{-1}$. (We note also that, if the cone angle *were* very narrow, transverse pressure gradients would cause significant departures from radial outflow; under these circumstances, the r-dependences would change, although the qualitative features would not be substantially altered.) We have purposely left out of our discussion any radiation from an external shock, which is expected to occur at radii beyond those considered here (and which can add other radiation components, especially a long term afterglow).

The standard internal shock model of GRB is generally assumed to produce its observed nonthermal radiation by the synchrotron (or possibly inverse Compton) process. Here, in addition to synchrotron we have also considered in more detail the role of the outflow photosphere and of possible nonthermal spectral distortions in it, as well as the role of pair breakdown in shocks with very high comoving luminosity. In a diagram (Figure 1) of radius vs. dimensionless entropy $\eta = \dot{L}/\dot{M}c^2$, the regions where the internal shocks are dominated by synchrotron radiation (and pair breakdown is unimportant, $\ell' \leq 1$) are shown by the vertically striped area S. The line where the compactness parameter $\ell' = 1$ runs parallel to the line $r_{ph}^{>}$ for the photosphere in the coasting regime, in the same figure. The region where internal shocks are dominated by pair-breakdown, $\ell' >$, is given by the horizontally striped region C in Figure 1, where the shock spectrum is dominated by comptonizing pairs. To the left and below the photospheric lines, shocks would occur at high optical depths and their spectrum would be thermalized, adding to the purely thermal (T) and non-thermal (PHC) components emerging form the photosphere. These various spectral components are shown in Figures 2 and 3 in a power per decade xL_x vs. x plot, where x is photon energy in electron rest mass units.

In our earlier papers on fireball shock models of GRB and most subsequent related work, the role of photospheres and pair breakdown was briefly considered, but until recently the observations

did not appear to provide much support for their being important. The need for a non-thermal spectrum continues to be a strong argument for shocks and a synchrotron component, while for the less problematic case of large baryon loads the photospheres occur in the coasting regime, where their observer frame thermal luminosity is drastically weakened by adiabatic cooling. This is confirmed by the spectra of Figures 2 and 3, where for moderate to large baryon loads (low η) and moderate variability $\xi_v \geq 10^2$ or $t_v \gtrsim 0.3$ s the thermal peaks T are strongly suppressed, especially in the more "conservative" region going part way above and below from the central and right-of-center panels of Figure 2. Pair breakdown is also a phenomenon considered in earlier papers (c.f. also Pilla & Loeb 1998, Papathanassiou & Mészáros 1996), which received less attention than it deserves because its importance appears to be restricted to a relatively narrow region of parameter space. This is illustrated in Figure 1, where one can compare the vertically striped region $\ell' < 1$ labeled S versus the narrowish horizontally striped region $\ell' > 1$ labeled C. This region would be even narrower if one normalized to $L_o \sim 10^{50}$erg s^{-1} as opposed to L_{52}.

However, fresh motivation for reconsidering the role of photospheres and pairs is provided by the evidence, in a non-negligible fraction of bursts, of low energy (1-10 keV) spectral slopes steeper than 1/3 in energy (or 4/3 in $\log xL_x$) and in some cases an X-ray excess above the power law extrapolation from higher energies, as well as the ubiquitousness of observed break energies clustering between 50-1000 keV (discussed in §1 and references there). A look at Figures 2 and 3 shows that allowing a larger role to photospheres and comptonized pairs provides a way of addressing these observational trends. If photospheres are rather more important than shocks (e.g. due to some preference for very high η, weakly varying outflows or low shock efficiencies) the thermal component can provide low energy slopes as steep as $\propto x^3$ in xL_x (while flatter slopes can be achieved through integration or distributions). The same can explain an X-ray excess well above the power law extrapolation from above. Reasonable break energies can be obtained from either the synchrotron or pair comptonization mechanisms in the shock, but they depend on $\Gamma = \eta$, and unless the range of η is narrow they would not necessarily cluster between 50-1000 keV. In the case of pair comptonization they also tend to be a bit high, unless the equilibrium pair temperature is $\Theta'_c \lesssim 0.03$. A preferred break could be attributed to a photospheric peak, provided baryon loads are very low, $\eta \geq \eta_* \sim 10^3$ in all cases; this still requires a strong shock synchrotron component, or possibly Alfvén wave comptonization in the photosphere, to explain the high energy power law spectra. It would also imply a pronounced upward change of slope above the break, from the thermal peak to a flatter power law in all bursts where a break is observed, unless the shock or Alfvén wave scattering always produces a luminosity comparable to the thermal photosphere. Preferred break energies arise naturally if Thompson's (1994) proposed mechanism of comptonization by Alfvén wave damping in the photosphere is taken at face value and has good efficiency, leading to a source frame break around 0.5 MeV. Note that the comptonized spectral slopes discussed here (either from thermal pairs in shocks or Alfvén waves in the photosphere) are nominally 1 and 0 in xF_x, but for simple time-dependent calculations an evolving slope is expected (e.g. Liang *et al.*, 1999, Thompson 1994). In reality the actual time dependence for an unsteady outflow leading to shocks, pair breakdown and comptonization could be more complicated.

If both a photospheric and a shock component are detected, one would expect the thermal photospheric luminosity (and its non-thermal part, if present) to vary on similar timescales as the nonthermal synchrotron or pair comptonized shock component (unless the shock efficiency is radius dependent, or unless one or both are beyond $r = r_o\eta^2$, in which case $r/c\eta^2$ imposes a lower limit on the corresponding variability timescale). But even if the bolometric luminosity varies on the same timescale, the luminosity in a given band (e.g. BATSE) probably varies differently, since the thermal peak energy is $\propto L^{1/4}$ and falls off steeply on either side, while the synchrotron peak energy varies $\propto B'\eta \propto L^{3/2}$ and falls off more slowly. The pair comptonized break energy on the other hand varies as $\eta \propto L$, and also drops off slowly on the low energy side, or on both sides if scattering off waves is present in the high energy side. If observations at high time resolution become possible in X-ray or optical during the burst (as opposed to the afterglow), we would expect (c.f. Figure 2) the bursts with shorter time structure (low ξ_v) to be more suppressed at these wavelengths, compared to those with longer variability timescales.

In summary, there are several plausible mechanisms for producing a preferred energy break, which rely on internal properties of the outflow. In those bursts with low energy slopes steeper than implied by synchrotron, the prominence of the photosphere is a likely explanation, in which case its luminosity could in some cases vary differently from the higher energy power law component. Intrinsically high luminosity bursts, where pair breakdown is inferred, would be predicted to have generally harder high energy power slopes than in lower luminosity bursts where synchrotron provides the high energy slope. If photospheric comptonization on Alfvén waves is responsible for the high energy power law slopes, the thermal peak and the power law should vary together in time. In this case a straightforward prediction is that the thermal peak photon energy and the intrinsic luminosity allow one to determine the expected maximum photon energy $x_w \sim \Gamma$.

This research has been supported by NASA NAG5-2857, NSF PHY94-07194 and the Royal Society.

REFERENCES

Brainerd, J. J., Preece, R., Briggs, M., Pendleton, G. & Paciesas, W., 1998, Ap.J., 501, 325

Cohen, E., Katz, J., Piran, T., Sari, R., Preece, R. & Band, D., 1997, Ap.J., 488, 330+.

Crider, A. *et al.*, 1997, Ap.J., 479, L39

Dermer, C.D., Böttcher, M., and Chiang, J., 1999, Ap.J., 515, L49

Eichler, D. & Levinson, A. 1999. Ap.J., subm. (astro-ph/9903103)

Ghisellini, G. & Celotti, A., 1999, Ap.J., 511, L93

Kumar, P, 1999, Ap.J.(Letters), in press (astro-ph/9907096)

Liang, E. P., 1997, Ap.J., 491, L15

Liang, E. P., Crider, A., Böttcher, M., and Smith, I., 1999, Ap.J., 519, L21

Mészáros , P., Laguna, P. & Rees, M.J. 1993 , Ap.J. 415, 181

Paczyński , B., 1986, Ap.J., 308, L43

Paczyński , B., 1990, Ap.J., 363, 218

Panaitescu, A., Spada, M. & Mészáros , 1999, ApJ(Lett.), in press (astro-ph/9905026)

Papathanassiou, H. & Mészáros , P, 1996, ApJ, 471, L91

Pilla, R. & Loeb, A., 1998, ApJ, 494, L167

Preece, R.D., *et al.*, 1998, Ap.J., 496, 849+.

Preece, R.D., Briggs, M., Mallozzi, G., Pendleton, G. & Paciesas, W., 1999, Ap.J.(Supp), in press (astro-ph/9908119)

Rees, M.J. & Mészáros , P, 1994, Ap.J., 430, L93

Shemi, A. & Piran, T., 1990, Ap.J., 365, L55

Svensson, R., 1987, MNRAS, 227, 403

Tavani, M, 1996, Ap.J, Ap.J., 466, 768

Thompson, C., 1994, MNRAS, 270, 480

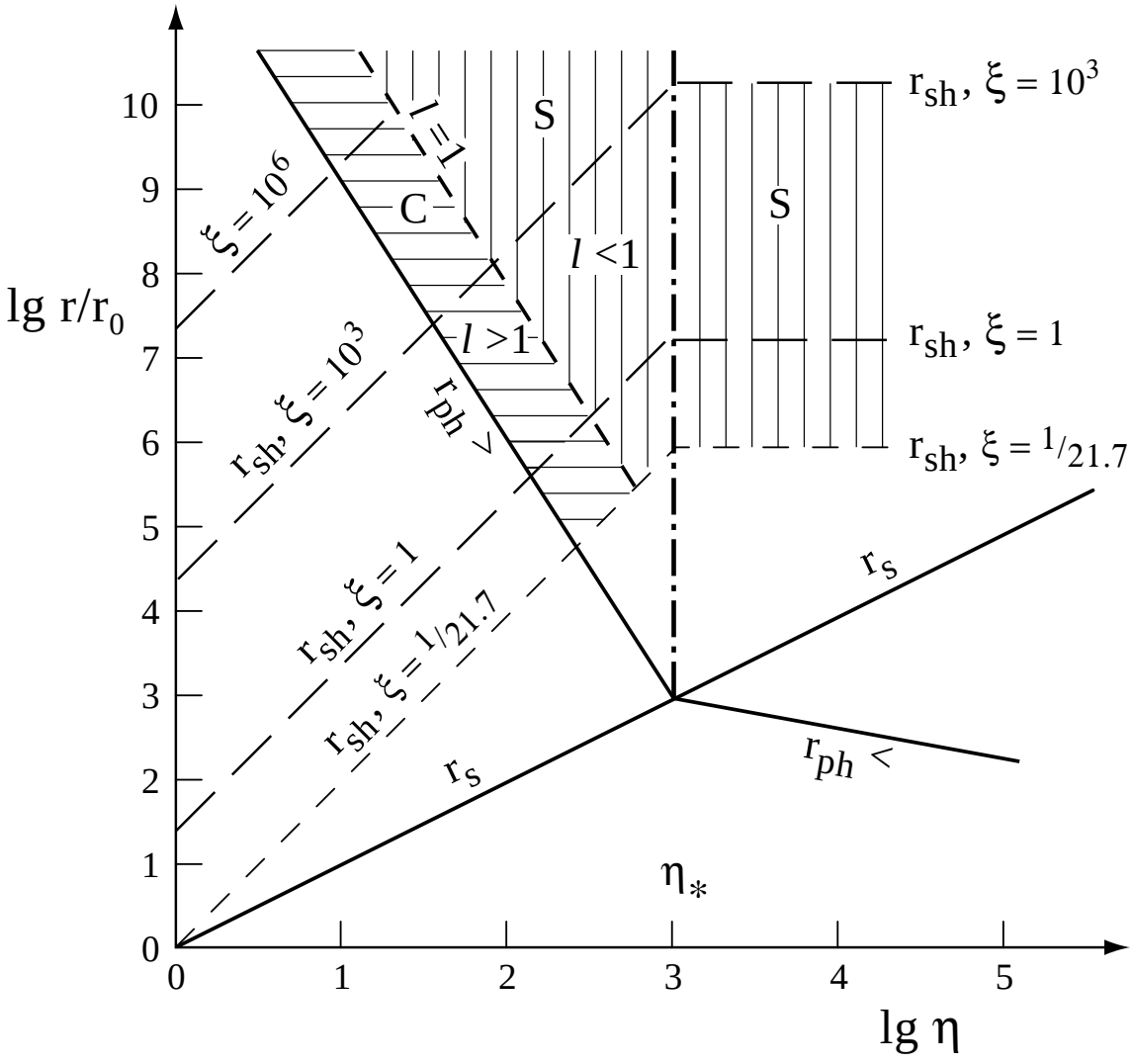

Fig. 1.— Radius vs. $\eta = L/\dot{M}c^2$ diagram showing the location of the photosphere r_{ph}, the saturation radius r_s, and the shock radii r_{sh} for various variability timescales ξ_v. The regions where the shock spectrum is dominated by synchrotron (S) or comptonization in a pair plasma (C) correspond to a comoving compactness $\ell' < 1$ or $\ell' > 1$.

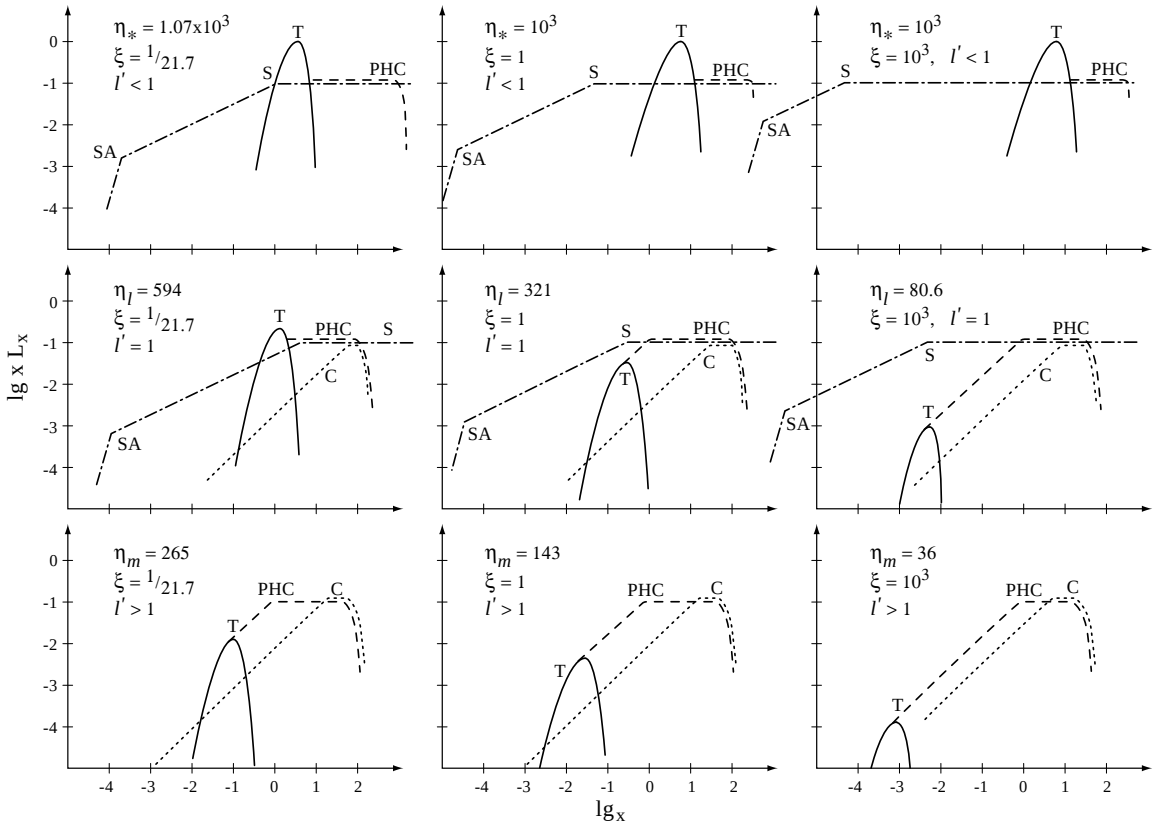

Fig. 2.— Luminosity per decade xL_x vs. $x = h\nu/m_e c^2$ for different values of η increasing upwards, and different variability timescales increasing to the right, using $\epsilon_w = \varepsilon_{sh} = 10^{-1}$. Pair formation is unimportant in the top row and important in the bottom row, being marginal in the middle row. T: thermal photosphere, PHC: photospheric comptonized component; S: shock synchrotron; C: shock pair dominated comptonized component.

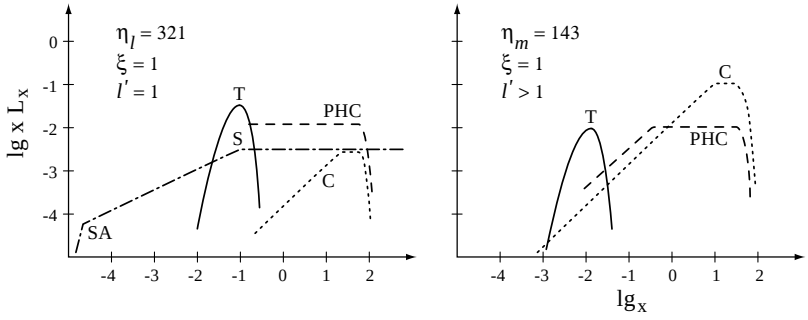

Fig. 3.— Luminosity per decade xL_x vs. x for two of the spectra in Figure 2 but with different shock synchrotron and pair comptonized components or lower comptonized photosphere component. Left panel: $\epsilon_w = 10^{-2}, \varepsilon_{sh} = 3 \times 10^{-3}$. Right panel: $\epsilon_w = 10^{-2}, \varepsilon_{sh} = 10^{-1}$.